Structured interactions drive abrupt transitions in the spatial organization of microbial communities

Mattia Mattei [1,*] David Soriano-Paños [1,2] Mahantesh Halappanavar [3] and Alex Arenas [1,3]
[1]*Departament d'Enginyeria Informàtica i Matemàtiques, Universitat Rovira i Virgili, 43007 Tarragona, Spain*
[2]*GOTHAM Lab, Institute for Biocomputation and Physics of Complex Systems, University of Zaragoza, 50018 Zaragoza, Spain*
[3]*Pacific Northwest National Laboratory, 902 Battelle Blvd, Richland, Washington 99354, USA*

(Received 23 July 2025; accepted 31 October 2025; published 24 November 2025)

Bacteria possess diverse mechanisms to regulate their motility in response to environmental and physiological signals, enabling them to navigate complex habitats and adapt their behavior. Some of these mechanisms are species specific and enable cells to modulate their movement based on the ecological identity of neighboring species. Here, we introduce a model in which bacteria interact via local signals that either enhance or suppress the motility of neighboring cells depending on species type. Through large-scale simulations and a coarse-grained stochastic model, we demonstrate the emergence of a sharp transition driven by nucleation processes: increasing the density of motility-suppressing interactions drives the system from a fully mixed, motile phase to a state characterized by large, stationary bacterial clusters. Remarkably, in systems with a large number of interacting species, this transition can be triggered solely by altering the structure of the motility-regulation interaction matrix while maintaining species and interaction densities constant. In particular, we find that heterogeneous and modular interactions promote the transition more readily than homogeneous random ones. These findings add a dimension to the theory of motility-induced phase separation and contribute to the ongoing effort to understand microbial interactions, suggesting that structured, nonrandom ones may be key to reproducing commonly observed spatial patterns in microbial communities.

DOI: 10.1103/g5bm-m9c4

I. INTRODUCTION

Microbial communities in natural environments frequently exhibit regular spatial organization, including the formation of dense surface-attached patches, multicellular aggregates, or flocks [1]. Spatial segregation among different microbial species is a pervasive phenomenon observed across diverse ecological contexts [2–5], yet the underlying factors and mechanisms responsible for generating such spatial heterogeneity are multifaceted and remain incompletely understood. Although it is well established that spatial patchiness can emerge spontaneously from growth and demographic fluctuations [6,7], comparatively less attention has been devoted to the role of active motility mechanisms in driving such spatial structuring. Indeed, a key aspect of bacterial adaptability is their capacity to regulate motility in response to a variety of external and internal signals. Mechanisms such as chemotaxis [8], sensing of physical and chemical cues, and regulatory networks, including intercellular communication systems like quorum sensing (QS) [9], allow bacteria to modulate gene expression and adjust their movement strategies accordingly. In many species, signals from QS or other pathways can lead to motility suppression, either through downregulation of flagellar genes or by promoting adhesive phenotypes that reduce mobility [10,11]. Yet signaling can also enhance motility, for instance, QS-dependent production of biosurfactants such as surfactin in *Bacillus subtilis* [12] putisolvins in *Pseudomonas putida* [13], and AHLs in *Rhizobium etli* [14] promotes swarming, surface spreading, or dispersal from microcolonies.

This connection between motility regulation and collective spatial organization has long been recognized in the field of active matter physics since the seminal work by Tailleur and Cates [15]. Here, they first demonstrated that run-and-tumble particles with density-dependent velocities, motivated exactly by quorum-sensing- or chemotaxislike regulation, can spontaneously segregate into dense and dilute phases, thereby introducing the concept of motility-induced phase separation (MIPS) [16]. Although MIPS was also shown to emerge from steric repulsion alone [17,18], more recently, Curatolo *et al.* [19] provided the first explicit incorporation of quorum sensing, showing both experimentally and theoretically that QS-regulated motility in engineered *E. coli* populations drives the formation of striking spatial patterns. Ridgway *et al.* [20] also explicitly included QS and demonstrated that intracellular feedback in QS-controlled motility can generate oscillatory instabilities. Extensions to multispecies systems have further enriched the picture: Dinelli *et al.* [21] showed that nonreciprocal motility-regulating interactions control the emergence of behaviors in two- and three-species systems, ranging from equilibriumlike coexistence to nonequilibrium dynamical patterns. Moreover, also Duan *et al.* [22] focused on two-species models, providing a detailed linear stability analysis and mapping out the conditions under which reciprocal and nonreciprocal couplings lead to distinct spatial instabilities.

*Contact author: mattia.mattei@urv.cat

While most theoretical studies have focused on simplified settings involving just few species, natural microbial communities typically consist of hundreds or even thousands of coexisting species that interact in complex and heterogeneous ways. Recently, Dinelli *et al.* [23] extended motility models to ecosystems with many interacting species, showing that both the strength and randomness of interspecies interactions drive the fragmentation of large communities into multiple coexisting clusters.

Here, we investigate how the phenomenology changes when motility-regulating interactions are not random but follow specific structures. With large-scale microscopic simulations, we find abrupt transitions from a well-mixed motile phase to a regime dominated by large stationary clusters as the density of motility-suppressing interactions increases, in line with the MIPS literature. To gain intuition, we develop an effective stochastic model in a simplified scenario involving just two species that identifies nucleation, namely the formation of stable clusters driven by fluctuations, as the key mechanism underlying this transition. Remarkably, we show that the same transition can arise solely from changes in the topology of the motility-regulation matrix, even when species abundances and the overall density of pairwise interactions are held constant. In particular, modular and heterogeneous matrices strongly promote spatial heterogeneity compared to random or homogeneous ones.

II. RESULTS

A. Microscopic model

We developed a microscopic simulation in which bacteria move according to run-and-tumble dynamics, consisting of ballistic motion at constant speed interrupted by random reorientations in two dimensions (see details in Sec. IV). Inspired by recent works [23,24], the velocity of each bacterium is modeled through a sigmoidal response function that modulates the local signals it receives from neighboring cells. The sigmoid provides a biologically plausible, saturating, monotone, and analytically tractable mapping from aggregated local signals to velocity magnitude. Specifically, the velocity of a particle i belonging to species S is given by

$$v_i = \frac{v_0}{1+\exp\left(-\frac{1}{k}\sum_{S'=1}^{N} A_{SS'}\,\phi_{S'}(i)\right)}, \qquad i \in S, \tag{1}$$

where v_0 is a fixed maximum velocity and the interaction matrix $A_{SS'}$ specifies how species S' influences the motility of species S, with positive values promoting and negative values suppressing movement. The local density $\phi_{S'}(i)$ denotes the concentration of species S' around particle i, and is computed by counting the number of particles of species S' within a fixed interaction radius R:

$$\phi_{S'}(i) = \frac{1}{\pi R^2}\sum_{j\in S'} M_{ij},$$

where $M_{ij} = 1$ if the Euclidean distance between particles i and j is less than R, and $M_{ij} = 0$ otherwise. The parameter k sets the density range over which cells are sensitive to motility regulation and it determines the steepness of the motility response. We will usually consider the limit $k \to 0$, in which the sigmoidal response becomes sharp and effectively switches between two states. In this regime, a global negative signal from the surrounding environment almost completely suppresses bacterial motility, while a slight global positive signal will automatically accelerate the bacterium's velocity to v_0. Larger values of k are considered in the Supplemental Material [25].

B. Two species setting

To gain intuition about the outcomes of the motility model above, we begin by analyzing a simplified case with only two species, a and b. A particularly illustrative scenario arises when bacteria of species a suppress each other's motility but experience enhanced motility in the presence of species b. In the sharp sigmoidal limit ($k \to 0$), this implies that a bacterium of species a will cease its motion whenever the local density of species a exceeds that of species b, and will resume movement once this condition is no longer met. This corresponds to setting the interaction matrix elements as $A_{aa} = -1$ and $A_{ab} = +1$. Moreover, we assume that bacteria of species b always move at a fixed velocity v_0; this can be achieved setting $A_{bb} = A_{ba} = +1$, which results in a always positive signal in a densely populated environment.

We are first interested in exploring how the number of nonmotile a-type bacteria at the steady state of the dynamics, hereafter denoted by $n_a^S(t^*)$, depends on the composition of the system. These nonmotile bacteria are those that, when the stopping criterion of our simulations is reached (Sec. IV), exhibit small and negligible velocities. For the simulations, we chose a scenario with $n = 16\,000$ bacteria in a $1\,\text{mm} \times 1\,\text{mm}$ quasi2D field. This corresponds to $\sim 0.016\,\text{cells}/\mu\text{m}^2$ (mean spacing $\sim 8\,\mu\text{m}$), i.e., a semidilute areal density consistent with many microfluidic assays. The interaction radius is set to $R = 25\,\mu\text{m}$ to represent an effective chemotactic/hydrodynamic neighborhood, and the maximum speed to $v_0 = 50\,\mu\text{m/s}$, typical for planktonic *Bacillus subtilis* swimmers and a commonly cited reference value [26,27]. Figure 1(a) shows that, as the population of species a increases relative to species b, the system exhibits an abrupt transition at a critical ratio: It shifts from a well-mixed state, where all a-type bacteria remain motile, to a phase in which large, stationary clusters of species a emerge. Note that the intermediate points in the critical region (in red) do not reflect partial stopping within individual simulations, but rather indicate that the transition occurs only in a subset of simulations, as shown in the inset of Fig. 1(a) for $n_a/n = 0.23$. The discontinuity of this transition is also confirmed by the presence of a pronounced hysteresis curve, which is detailed in the Supplemental Material [25].

Fig. 1(b) displays the time evolution of the fraction of motile bacteria in a representative simulation performed in the critical region, showing how, after a transient phase, a nucleus spontaneously forms and attracts the accumulation of all bacteria. This phenomenology is observed across various combinations of radii and velocities (see the Supplemental Material [25]). These empirical observations of the temporal dynamics for the number of nonmotile bacteria suggest that the transition is driven by a stochastic nucleation process, a mechanism widely recognized as the trigger for first-order phase transitions in condensed matter and even in biological

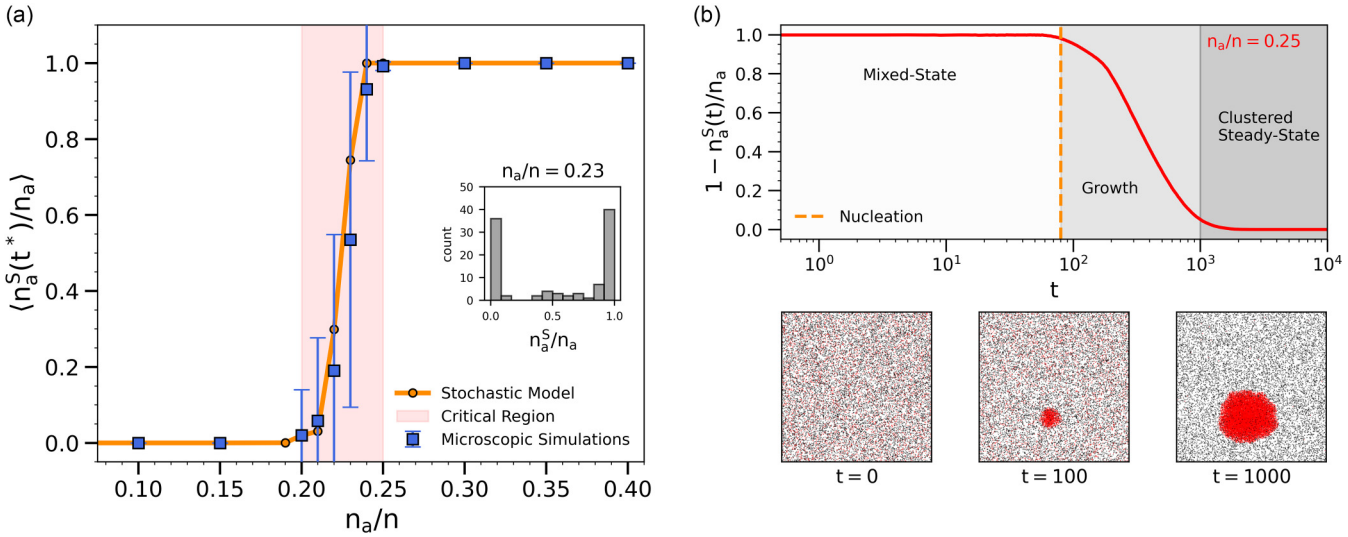

FIG. 1. (a) Mean fraction of a-type nonmotile bacteria at the end of the simulations ($\langle n_a^S(t^*)/n_a \rangle$) as a function of the fraction of bacteria belonging to species "a" (n_a/n). Blue squares indicate the mean values from 100 runs of the microscopic simulation, with error bars representing standard deviations. The orange line shows results obtained from the mean of 100 realizations of the theoretical stochastic model simulated using the Gillespie algorithm. The "critical" region, where the transition may stochastically occur or not, is highlighted in slight red. The inset shows the distribution of the results for each of the 100 simulations for $n_a/n = 0.23$. All the simulations here are performed with a total number of bacteria $n = 16\,000$, an interaction radius of $R = 25$ μm and a maximum velocity $v_0 = 50$ μm/s. (b) Top: temporal dynamics of the fraction of motile bacteria $n_a^S(t)$ from a representative run of the microscopic simulation at $n_a/n = 0.25$. Bottom: graphical representations of the system at three different time steps, highlighting the nucleation process. Bacteria of species "a" and "b" are depicted in red and black, respectively.

systems as well [28]. Specifically, in the vicinity of the critical region, the system exhibits a finite probability of spontaneously forming a stable, immobile cluster of species a. In this context, "stable" indicates that the cluster has reached a sufficiently high density such that the probability of bacteria within it regaining the conditions necessary to resume motility becomes very low. This localized cluster acts as a nucleation seed, triggering the irreversible arrest of motility in nearby particles and eventually propagating throughout the system. The emergence of such nuclei is a rare event in the well-mixed phase, but once formed, they grow by recruiting neighboring particles, leading to the abrupt macroscopic transition.

To support this interpretation, we developed a coarse-grained stochastic description that explicitly accounts for the size and number of stationary clusters, along with their probabilities to form, grow, or shrink. This type of effective, mesoscopic description is commonly used in the study of nucleation phenomena [29,30]. We consider the following stochastic events: (i) motility loss, $m \to s$: when a bacterium transitions from the freely moving planktonic state to a nonmotile state; (ii) motility gain, $s \to m$: when a stationary bacterium fulfills the conditions to resume motion; (iii) cluster growth, $C_i + m \to C_{i+1}$: when a motile bacterium joins a stationary cluster of size i, increasing its size to $i + 1$; (iv) cluster fission, $C_i \to C_{i-1} + m$: when a stationary cluster loses one of its bacteria, which then becomes motile again. In these processes, C_i denotes a stationary cluster of size i of bacteria of species a (for simplicity, we omit the species index in the equations), and the notations m and s refer to single motile or not motile bacteria, respectively, not currently part of any cluster. The reaction rates associated with these transitions, along with the corresponding master equation, are derived in detail in Sec. IV. The orange curve in Fig. 1(a) shows the results averaged over multiple stochastic realizations of the model generated using the Gillespie algorithm [31]. These results closely reproduce the behavior observed in the microscopic simulations, thus proving that the stochastic mesoscopic description of the dynamics of clusters can sucessfully capture the emergent phenomena from the microscopic interactions.

C. Large communities

We now generalize our formalism to ecosystems with $N > 2$ distinct species considering that each element $A_{SS'}$ of the $N \times N$ interaction matrix encodes how species S' influences the motility of species S. This formalism permits the inclusion of specific structural properties, depending on which model is chosen to generate the matrix. To set a baseline scenario, we start by assuming that motility-suppressing interactions are randomly distributed, so that each species experiences, on average, the same number of such interactions. This graph-construction method, known as the Erdős-Rényi (ER) model [32], produces an interaction matrix lacking inherent structural correlations (see Sec. IV for details). Specifically, for a fixed number of motility-suppression interactions L_-, we choose randomly pairs of species S and S' and set $A_{SS'} = -1$, assuming that both species suppress each other's motility. Then, to simplify the framework, we defined its dual as representing motility enhancement, setting the remaining entries to $+1$. This ensures that all interactions are exclusively suppressive or enhancing.

Figure 2 shows that, under this configuration, simulations with $N = 100$ different species display phenomenology

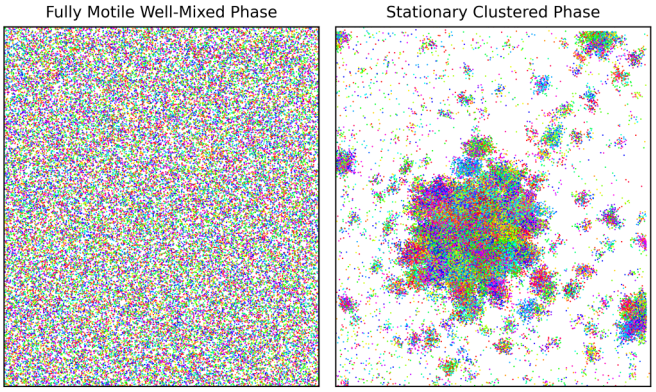

FIG. 2. Steady-state spatial configurations of $n = 100\,000$ bacteria partitioned into $N = 100$ different species, shown for two distinct values of the number of motility suppression links. When the number of suppression links is insufficient, the system remains in a fully motile, well-mixed phase. Upon reaching a critical value, the system may undergo a transition to a stationary clustered state in which all bacteria cease motion. Simulations are performed with $R = 10$ μm and $v_0 = 50$ μm/s within a two-dimensional box of size $[0, 1]$ mm $\times$ $[0, 1]$ mm.

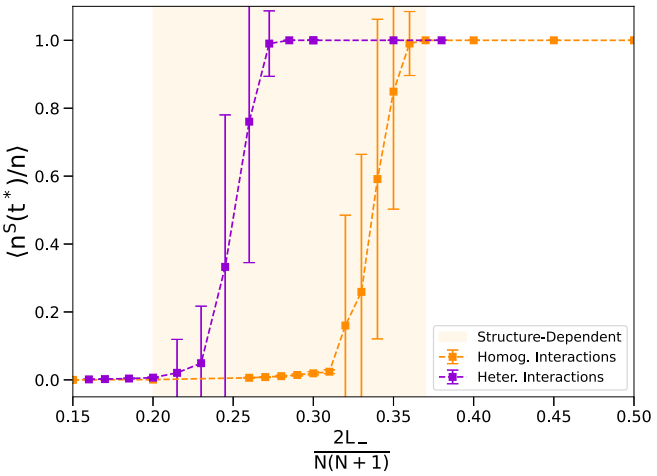

FIG. 3. Mean fraction of nonmotile bacteria at equilibrium n^S/n as a function of the density of species-specific motility suppression interactions $2L_-/(N(N+1))$. The orange and the violet curves correspond to a homogeneous interaction matrix generated by the ER model and a heterogeneous one provided by the Barabási-Albert (BA) model. Dots indicate averages over 100 independent microscopic simulations, with error bars representing standard deviations. Therefore, each data point corresponds to 100 different graph realizations, all sharing the same mean number of interactions and the same structural type under consideration (random or heterogeneous). The yellow region highlights the domain where the system's phase depends solely on the structure of the interactions matrix. All simulations are performed within a two-dimensional box of size $[0, 1]$ mm $\times$ $[0, 1]$ mm and with $n = 100\,000$ bacteria, $N = 100$ species, $R = 10$ μm, and $v_0 = 50$ μm/s.

analogous to that observed in the two-species scenario, characterized by a sharp transition between a well-mixed motile phase and a stationary clustered phase, wherein bacteria of all species lose motility. Here, the control parameter shifts from species abundances to the density of motility suppression interactions, $2L_-/(N(N+1))$, see Fig. 3. Therefore, increasing the proportion of suppression links in multispecies communities drives the system toward configurations where nucleation events are more likely, consequently promoting the emergence of the transition toward the nonmotile phase.

We then examined whether particular structures in the interactions matrix could modulate the previously observed behavior. In particular, we considered more heterogeneous matrices, where a few species engage in many interactions while the majority interact with only a few, as well as modular matrices, where species are organized into distinct groups with dense interactions within each group and sparse interactions between groups. These structured patterns in the interaction matrix are relevant because microbial systems frequently exhibit either heterogeneity or modularity in their interspecies interactions. In Fig. 3, we present a comparison between homogeneous matrices generated by the ER model and more heterogeneous ones produced using the Barabási-Albert (BA) model [33]. The BA model generates graphs with power-law degree distributions by iteratively adding nodes according to a preferential attachment mechanism, whereby nodes are more likely to connect to existing nodes with higher degrees (see more details in Sec. IV). Figure 3 shows how, in the case of heterogeneous interactions, the critical point of the transition falls much earlier respect to the case of homogeneous ones, highlighting a region (shadowed region in Fig. 3) in which changing the structure of the interaction matrix can lead to distinct asymptotic states (the motile, well-mixed phase or the stationary clustered one), even under the same global number of interactions. This earlier onset of the transition can be attributed to hub species, those with many motility-suppression interactions, which are more probable to act as nucleation seeds and thereby trigger the transition (see Sec. 2 of the Supplemental Material [25]).

To investigate the impact of modular structure in the interaction matrix, we employed a simplified version of the stochastic block model (SBM) [34]. Specifically, we assume that species are partitioned into g distinct communities or groups, with a probability p_{in} of establishing motility-suppressing interactions between species within the same group, and a probability p_{out} of connecting to species in other groups. Configurations where $p_{\text{in}} \gg p_{\text{out}}$ correspond to highly modular interaction matrices, whereas the limit $p_{\text{in}} \approx p_{\text{out}}$ recovers a homogeneous one (more details in Sec. IV). In Fig. 4, we set $g = 4$ and examine the fraction of bacteria that become nonmotile at equilibrium in a range of p_{in} and p_{out} values for the motility suppression matrix. Interestingly, our results indicate that interactions matrix with pronounced modularity facilitate the transition with substantially fewer suppression interactions: increasing the density of intragroup interactions while keeping the overall density of interaction constant allows transition between the motile and the stationary cluster phases. This likely reflects that partitioning species into well-defined communities in the interaction matrix promotes the compartmentalization and clustering of bacteria in space (see Sec. 2 of the Supplemental Material [25]).

Taken together, both results show how the latter transition is given not only by the overall density of motility-suppressing

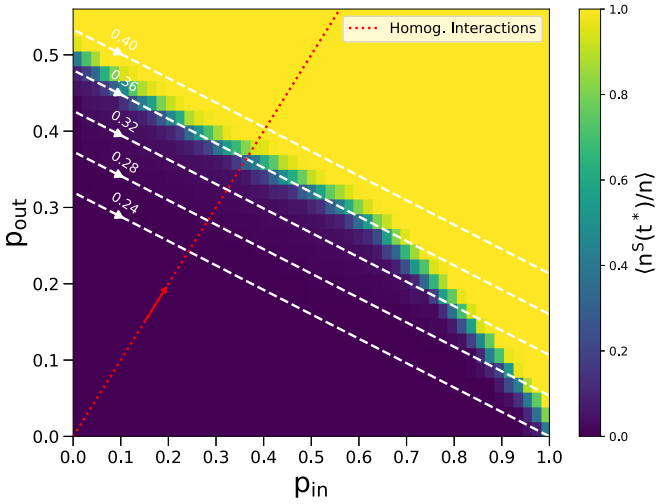

FIG. 4. Heatmap showing the average number of nonmotile bacteria at equilibrium for modular motility suppression matrices generated using an SBM. The x axis represents p_{in}, the probability of forming interactions within groups, while the y axis corresponds to p_{out}, the probability of establishing interactions between different groups. We set the number of species' groups to $g = 4$. White dashed lines denote curves of constant interactions density, indicating configurations with identical numbers of interactions but different combinations of p_{in} and p_{out}. The red dotted line represents the scenario of fully homogeneous interactions, where $p_{\text{in}} = p_{\text{out}}$. A step size of 0.02 was used for both p_{in} and p_{out}, and each grid cell displays the mean value computed from 100 independent microscopic simulations.. All simulations were conducted within a two-dimensional domain of size $[0, 1]\,\text{mm} \times [0, 1]\,\text{mm}$, with $n = 100\,000$ bacteria, $N = 100$ species, $R = 10\ \mu\text{m}$, and $v_0 = 50\ \mu\text{m/s}$.

interactions but also depends on the underlying structure of the interaction matrix.

III. DISCUSSION

In this study, we have shown that a minimal model incorporating local, species-specific modulation of motility can robustly reproduce the patchy spatial structures commonly observed in microbial communities. A key insight from our analysis is the identification of nucleation as the fundamental mechanism seeding the formation of such patterns, suggesting its potential relevance in contexts such as biofilm development [35–37]. Beyond this mechanistic aspect, we found that the structure of the interaction matrix plays a decisive role: modular and heterogeneous topologies facilitate the emergence of spatial organization far more effectively than random, unstructured ones. Several studies have underscored the importance of chemotaxis and other directed movement behaviors in reproducing specific microbial spatial patterns [38,39]. However, to our knowledge, only recent studies [23,40] have directly investigated how species-specific interactions in multispecies systems can modulate bacterial motility, although without addressing the specific structure of the underlying interaction matrix. More similar in spirit to this work is the study by Diego *et al.* [41], which specifically addresses the role of network topology in the formation of spatial patterns, although in the context of reaction-diffusion systems and Turing patterns rather than MIPS-like dynamics.

Our findings are especially meaningful because motility-regulating interactions can serve as proxies for broader ecological interactions. Indeed, it is reasonable to expect that species favor spatial proximity when mutualistic or otherwise cooperative interactions provide reciprocal benefits, and, conversely, competitors tend to segregate in space. A common theoretical approach has been to model such general ecological interactions with random matrices [42,43]. However, a growing body of empirical and experimental work indicates substantial structure: Co-occurrence analyses frequently reveal heavy-tailed degree distributions and modular organization [44–46], and laboratory studies of resource competition and metabolic crossfeeding likewise support modular interaction architectures in microbial communities [47,48]. These observations are consistent with the findings of this work, as we showed that structured interactions favor the emergence of widespread spatial patterns.

We are aware of the multiple limitations of our theoretical framework. Building coarse-grained descriptions for the vast and complex world of the microbiome inevitably means leaving many aspects behind. First, we described mechanisms that regulate motility in bacteria through the production, diffusion, and detection of small molecules, but we did not explicitly include these detailed processes in the model. In our framework, the neighbor count within radius R should be interpreted as a proxy for the effective concentration of molecules perceived by a cell after diffusion, decay, and uptake. This is, of course, a strong abstraction, but considering that bacterial interactions are often short ranged [49–51], combined with the high densities used in our simulations (up to 100 000 cells in the multispecies case), the additional "noise" from spatial diffusion and signal detection is likely negligible for the purposes of this study. We therefore believe that explicitly modeling the biochemical processes would not change the qualitative nature of our findings for the questions addressed here.

Another strong approximation is to represent the effect of one species on the motility of another as a fixed entry in a stationary interaction matrix. We are aware that, in reality, these interactions are highly variable and context dependent. However, our goal was not to provide a universal description of all possible interaction modes, but rather to investigate what happens once a particular set of interactions is established, always considering the same scenario across simulations. In addition, since we focus deliberately on shorter timescales, we believe that the variability of interactions can be reasonably relaxed and captured by fixed quantities.

Moreover, our model employs a two-dimensional approximation to systems that are intrinsically three dimensional [52]. While this simplification is appropriate for the early stages of surface colonization, when cells remain confined to a thin monolayer [53], future extensions to fully three-dimensional geometries will be valuable for testing our predictions in more realistic biofilm environments.

Finally, in the Supplemental Material [25] we showed that the phenomenology we observe is not exclusive to the limit $k \to 0$, but remains robust also for larger values of k. In this sense, we want to stress that considering a small k does not unrealistically boost the efficiency of bacteria to uptake

signaling molecules; instead, it simply reflects the assumption that even a single emitting source cell can potentially generate enough signal to induce a motility change up to the edge of the sensing radius. From this perspective, a small k is not necessarily coupled with a small R, since k only governs the intracellular sharpness of the response.

In conclusion, the abrupt transition we have observed represents a distinctive example of motility-induced phase separation (MIPS). Unlike conventional MIPS, typically driven by changes in global density or motility parameters, our results demonstrate that similar phase transitions can emerge solely through alterations in the structure of the interspecies interactions matrix. These insights highlight the potential for matrix topology itself to act as a critical determinant of large-scale spatial organization in microbial ecosystems.

IV. METHODS

A. Coarse-grained stochastic model

We consider the simplified scenario described as the "two-species setting" in the main text, consisting of two species, a and b. Recall that bacteria belonging to species a can suppress each other's motility, potentially leading to the formation of stationary clusters, whereas bacteria of species b remain motile at a constant speed v_0.

We describe mesoscopically the system of bacteria of species a by the state vector

$$\mathbf{n}(t) = (n_0(t),\, n_1(t),\, n_2(t),\, \ldots,\, n_{n_a}(t)),$$

where n_0 denotes the number of free motile bacteria and n_i (for $1 \leqslant i \leqslant n_{n_a}$) denotes the number of clusters composed of i nonmotile bacteria. Let $P(\mathbf{n}, t)$ denote the probability that the system occupies state $\mathbf{n}$ at time t. To define the stochastic dynamics, we identify the possible transitions between different states of the vector and their associated rates.

Motility loss ($0 \to 1$). Consider a motile a-type bacterium i. In the limit $k \to 0$ of the sigmoid function defining the velocity [Eq. (1)], bacteria of species a can suppress their motility when the number of nearby bacteria of species a exceeds that of the motility-enhancing bacteria of species b within a neighborhood of radius R. In a well-mixed system, the numbers of species a and b bacteria inside a circle of radius R centered at the position of the bacterium i, denoted by $n_a^R(i)$ and $n_b^R(i)$, respectively, are Poisson distributed with means $\lambda_a = \pi R^2 n_a$ and $\lambda_b = \pi R^2 n_b$. For the sake of clarity, from then on, we will omit the notation (i).

For the bacterium i to transition from a motile to a nonmotile state during a time step Δt, it must experience a change from $n_a^R(t) \leqslant n_b^R(t)$ to $n_a^R(t+\Delta t) > n_b^R(t+\Delta t)$. Such a transition can occur either through the entry of additional species a bacteria into the neighborhood or through the exit of species b bacteria from the same region. If we consider sufficiently small time steps, it is sufficient to account only for events involving the entry of a single bacterium of species a into the neighborhood or the exit of a single bacterium of species b. Under these conditions, the relevant transition corresponds to a change from $n_a^R(t) = n_b^R(t)$ to $n_a^R(t+\Delta t) = n_b^R(t+\Delta t) + 1$.

The probability that a bacterium of species a enters the neighborhood of the bacterium i during the time interval Δt can be expressed as the product of two factors. First, the probability that another motile bacterium of species a is located within the annular shell $[R, R + v_0\Delta t]$ at time t, and second, the probability that it moves inward across the boundary into the region of radius R around i. The probability of finding a motile bacterium of species a within the shell is given by the product of the density n_0/A and the shell's area, which is

$$\pi(R + v_0\Delta t)^2 - \pi R^2 \approx 2\pi R v_0 \Delta t + o(\Delta t^2).$$

Given the smallness of $v_0\Delta t$, the probability that the bacterium moves inward across the area can be taken as $1/2$, as the annular shell is restricted to the circle perimeter. Therefore, the overall probability for the entry of a single motile species a bacterium into the neighborhood during Δt is

$$P^a_{\text{entry}} \approx n_0 \pi R v_0 \Delta t,$$

where we recalled that $A = 1$. For a bacterium of species b, the probability of either entering or exiting the neighborhood during a time interval Δt is also given by

$$P^b_{\text{entry}} = P^b_{\text{exit}} \approx n_b \pi R v_0 \Delta t,$$

since these bacteria move continuously at a constant speed v_0 in random directions, so that the in- and out-fluxes are the same.

The combined probability of either a species a bacterium entering the neighborhood or a species b bacterium exiting it must be multiplied by the probability that, at time t, the local populations satisfy $n_a^R(t) = n_b^R(t)$. This probability is given by

$$P\big(n_a^R = n_b^R, t\big) = \sum_{n_a^R(t)=1}^{n_a} P\big(n_a^R(t)\big)\, \frac{P\big(n_b^R(t) = n_a^R(t)\big)}{P\big(n_b^R(t) \geqslant n_a^R(t)\big)},$$

where $P(n_a^R(t))$ and $P(n_b^R(t))$ are the Poisson's distributions for the local populations of a-type and b-type bacteria. The division by $P(n_b^R(t) \geqslant n_a^R(t))$ arises because $n_b^R(t)$ must be at least equal to $n_a^R(t)$, otherwise, bacterium i would already have transitioned to a nonmotile state. Substituting the Poisson's distributions, we obtain

$$P\big(n_a^R = n_b^R, t\big) = \sum_{n_a^R(t)=1}^{n_a} \sum_{n_b^R \geqslant n_a^R} \frac{e^{-\lambda_a}\, \lambda_a^{n_a^R} \lambda_b^{n_a^R - n_b^R}\, n_b^R!}{\big(n_a^R!\big)^2},$$

where, for clarity, the time argument has been omitted in the right term of the equation. Finally, the total rate $W_{0\to1}$ for unit of time at which free bacteria of species a lose motility is just given by

$$\begin{aligned} W_{0\to1} &= \frac{n_0}{\Delta t}\left(P\big(n_a^R = n_b^R\big)\left(P^a_{\text{entry}} + P^b_{\text{exit}}\right)\right) \\ &= n_0 \pi R v_0 \left(P\big(n_a^R = n_b^R\big)\left(n_0 + n_b\right)\right). \end{aligned} \tag{2}$$

Motility gain ($1 \to 0$). The derivation of the motility gain rate follows a similar procedure as in the previous section. Here, the relevant transition during a sufficiently small time step is the change from $n_a^R(t) = n_b^R(t) + 1$ to $n_a^R(t+\Delta t) = n_b^R(t+\Delta t)$. This transition can occur either through the entry of a bacterium of species b into the circle of radius R surrounding the considered nonmotile bacterium i or through the exit of a free bacterium of species a from that region. Therefore,

we consider the probability

$$P\big(n_a^R = n_b^R + 1, t\big) = \sum_{n_a^R(t)=1}^{n_a} P\big(n_a^R(t)\big) \frac{P\big(n_b^R(t) = n_a^R(t) - 1\big)}{P\big(n_b^R(t) < n_a^R(t)\big)},$$

where the denominator serves as a normalization factor because, at time t, it must hold that $n_b^R(t) < n_a^R(t)$ for bacterium i to remain in a nonmotile state. The total transition rate $W_{1\to 0}$, representing the probability per unit time that nonmotile bacteria of species a regain motility, is then given by

$$\begin{aligned} W_{1\to 0} &= \frac{n_1}{\Delta t}\left(P\big(n_a^R = n_b^R + 1\big)\left(P_{\text{entry}}^b + P_{\text{exit}}^a\right)\right) \\ &= n_1 \pi R v_0 \left(P\big(n_a^R = n_b^R + 1\big)\big(n_0 + n_b\big)\right). \end{aligned} \tag{3}$$

Cluster growth ($C_i \to C_{i+1}$). We assume that each bacterium occupies a circular area with diameter d, representing its physical size and that clusters are perfect circles with radius R_C. Thus, the total area occupied by i bacteria is given by $A(i) = i\pi d^2/4$. If i nonmotile bacteria of species a are arranged in an optimal hexagonal close packing, the cluster can be approximated by a single circular region with effective area $A_{C_i} = A(i)/\eta$, where $\eta = \pi/(2\sqrt{3})$ denotes the packing efficiency of hexagonal close packing. The corresponding cluster radius is therefore $R_{C_i} = d\sqrt{i\sqrt{3}/2\pi}$. For a cluster to grow, a motile bacterium of species a must collide with the interaction zone surrounding the cluster. This interaction area has a radius $R + R_{C_i}$, yielding a total cross-sectional area of $\pi(R + R_{C_i})^2$. As before, we consider small time steps Δt and assume only one collision event per interval. The relevant shell region is defined by $[R + R_{C_i},\ R + R_{C_i} + v_0\Delta t]$, whose area is approximately $2\pi v_0 \Delta t(R + R_{C_i}) + o(\Delta t^2)$. Assuming that the probability for a bacterium in this shell to move inward is again $1/2$, the probability that a motile bacterium of species a enters the interaction region during Δt is given by $P_{\text{entry}}^a = n_0 \pi v_0 (R + R_{C_i})\Delta t$. The corresponding total cluster growth rate per unit time, $W_{C_i\to C_{i+1}}$, for clusters of size i is therefore

$$\begin{aligned} W_{C_i\to C_{i+1}} &= n_i\, n_0\, \pi\, v_0 \big(R + R_{C_i}\big) \\ &= n_i\, n_0\, \pi\, v_0 \left(R + d\sqrt{\frac{i\sqrt{3}}{2\pi}}\right). \end{aligned} \tag{4}$$

Cluster fission ($C_i \to C_{i-1}$). Clusters can subsequently lose bacteria due to collisions with b-type bacteria. Consider a bacterium situated at the perimeter of a cluster with radius R_{C_i}. If $R_{C_i} \leqslant R/2$, this bacterium interacts with the entire cluster, otherwise, it interacts only with a fraction α of it. To compute α, we calculate the area of intersection between the circular interaction zone of radius R centered on the edge bacterium and the cluster area A_{C_i}. This intersection area is given by [54]

$$\begin{aligned} A_\cap = R_{C_i}^2 \cos^{-1}\left(1 - \frac{R^2}{2R_{C_i}}\right) + R^2 \cos^{-1}\left(\frac{R}{2R_{C_i}}\right) \\ - \frac{1}{2}R\sqrt{4R_{C_i}^2 - R^2}, \end{aligned}$$

so that we approximate $\alpha = A_\cap/A_{C_i}$, when $R_{C_i} > R/2$, otherwise $\alpha = 1$. Thus, a bacterium at the cluster boundary experiences a local number of suppression interactions $n_a^R = \alpha i + n_a^{R,o}$, where $n_a^{R,o}$ represents interactions with other motile a-type bacteria located outside the cluster. Consider the case where, at time t, the condition $n_B^R(t) = n_a^R(t) - 1 = \alpha i + n_a^{R,o} - 1$ holds. If a b-type bacterium collides with the area of radius $R_{C_i} + R$, or if a free a-type bacterium exits the shell defined by $[R_{C_i}, R_{C_i} + R]$, the bacterium at the boundary can regain motility. Using a reasoning analogous to previous derivations, the total rate at which clusters of size i lose bacteria is given by

$$\begin{aligned} W_{i\to i-1} = n_i \pi v_0 \big(R_{C_i} + R\big) \sum_{n_a^{R,o}} P\big(n_a^{R,o}\big) \\ \times \frac{P\big(n_B^R = n_a^{R,o} + \alpha i - 1\big)}{P\big(n_B^R < n_a^{R,o} + \alpha i\big)} (n_0 + n_B), \end{aligned} \tag{5}$$

where $n_a^{R,o}$ is assumed to be Poisson-distributed, exactly as n_a^R.

Master equation. The time evolution of $P(\mathbf{n}, t)$ can be described by

$$\begin{aligned} \frac{d}{dt}P(\mathbf{n}, t) = \sum_r [W_r(\mathbf{n} - \Delta\mathbf{n}_r)\, P(\mathbf{n} - \Delta\mathbf{n}_r, t) \\ - W_r(\mathbf{n})\, P(\mathbf{n}, t)], \end{aligned} \tag{6}$$

where $r \in \{0 \to 1,\ 1 \to 0,\ C_i \to C_{i\pm 1}\}$, with corresponding updates to $\mathbf{n}$. This stochastic dynamics is solved via the Gillespie algorithm, yielding trajectories that match the microscopic simulations (Fig. 1 and the Supplemental Material [25]).

B. Network models

To explore how different interactions matrix structures affect the phenomenology of the motility model, we generated interaction matrices using three standard models from network theory: ER, BA, and SBM. Each model introduces distinct structural properties, allowing us to disentangle the role of randomness, heterogeneity, and modularity in shaping community-level outcomes.

Erdős-Rényi (ER). The ER model [32] is the simplest random graph construction. In its classical version, given N nodes, each of the $\frac{N(N+1)}{2}$ possible edges, including pairs of nodes and self-loops, is independently included with probability p. This leads to an expected number of links given by $\langle L_- \rangle = pN(N+1)/2$. In our case, we consider a prescribed connectivity of $2L_-/(N(N+1))$ motility-suppressing interactions, we randomly sample pairs of species S and S' and set the corresponding entry to 1. We repeat this process until L_- links are established.

Barabási-Albert (BA). The BA model [33] introduces heterogeneity by generating scale-free networks through preferential attachment. We initialize from a seed graph G_0 with N_0 nodes and L_0 edges (in our case, the largest connected component of an ER graph with 30 nodes and connection probability $p = 0.2$). Nodes are then added sequentially until reaching the target size N. Each added node introduces exactly m edges, which connect to existing nodes with probability proportional to their degree. Specifically, the probability that

an edge attaches to node i is given by

$$\Pi(i) = \frac{k_i}{\sum_j k_j},$$

where k_i is the degree of node i at the time of attachment.

The expected total number of edges at the end of the construction is

$$\langle L_- \rangle \;=\; \tfrac{1}{2}\, p N_0(N_0 - 1) \;+\; m\,(N - N_0).$$

After fixing this target, we adjusted the parameter m to generate networks with the desired connectivity. This construction produces heterogeneous interaction matrices, where a few hub species acquire very high degree, while most species remain sparsely connected. In the standard BA model, the resulting degree distribution follows a power law

$$P(k) \sim k^{-\gamma}, \quad \gamma \simeq 3.$$

As the last step, we add each of the N possible self-loops with a probability $p_{\text{self}} = 2\langle L_- \rangle / [N(N-1)]$.

Stochastic Block Model (SBM). The SBM [34] provides a flexible framework to encode modular structure. We partition the N species into g groups of equal size $n_g = N/g$. In our simulations, we have considered $g = 4$ groups with $n_g = 25$ species. In its most general form, the model is defined by a full $g \times g$ matrix of edge probabilities specifying the likelihood of interactions between each pair of groups. Here, we considered a simplified but widely used version in which only two probabilities are introduced: p_{in} for within-group interactions and p_{out} for between-group interactions. The expected total number of edges is then

$$L_- = \tfrac{1}{2}\big[p_{\text{in}}\, n_g(n_g - 1)g \;+\; p_{\text{out}}\, g(g-1)n_g^2\big], \qquad (7)$$

so that we can obtain networks with different link densities varying only p_{in} and p_{out}. When $p_{\text{in}} \sim p_{\text{out}}$, the algorithm generates graphs equivalent to the Erdős-Rényi case, while for $p_{\text{in}} \gg p_{\text{out}}$ it produces strongly modular structures.

All three algorithms produce adjacency matrices with entries equal to either 0 or 1. To connect this representation to our motility framework, we mapped the values as follows: Entries equal to 1 were replaced by -1 to denote motility-suppressing links, while entries equal to 0 were replaced by $+1$ to represent motility-enhancing interactions.

C. Simulation details

All simulations, both the microscopic and the Gillespie-based ones, incorporate a stopping criterion: the coefficient of variation of the number of nonmotile bacteria must fall below 0.001 over the last 500 time steps. If this condition is not satisfied, the simulation is terminated after a total of 5000 time steps. When we refer to the number of bacteria that stop their motion, we are actually counting bacteria with velocity dropped below 10^{-5} μm/s, as the sigmoid function never really touches exactly zero.

The microscopic simulation scripts are implemented in C++. To efficiently compute the number of interacting bacteria, the algorithm constructs a data structure known as a random geometric graph [55], which is updated in parallel at each time step. The parallelization leverages spatial discretization, dividing the domain into squares of side length R. To identify potential neighbors, each bacterium only checks distances to others located within its own cell and the surrounding eight neighboring cells. To avoid introducing correlations in bacterial trajectories, tumbling times t—the times at which bacteria change their movement direction—are sampled from an exponential distribution given by $p(t) = e^{-t/\tau_0}$ with $\tau_0 = 1$. At each simulation time step, the number of neighbors for each bacterium is first computed, which determines its instantaneous velocity v_i. A fully random movement direction is then selected. If the next tumbling event is predicted to occur within the current time interval $[t, t + \Delta t]$, the bacterium moves up to that tumbling time, after which another direction is sampled. This process repeats until the full time step Δt is completed.

ACKNOWLEDGMENTS

The authors acknowledge Julien Tailleur for his insightful suggestions and for providing valuable guidance to relevant literature. This work has been supported by MCIN/AEI/10.13039/501100011033 and by the European Regional Development Fund (ERDF) "A way of making Europe," Grant No. PID2021-128005NB-C21, Generalitat de Catalunya (2021SGR-00633), Universitat Rovira i Virgili (2023PFR-URV-00633), and the European Union Horizon Europe Programme under the CREXDATA project (Grant Agreement No. 101092749), and in part by the Laboratory Directed Research and Development Program at the Pacific Northwest National Laboratory (PNNL). A.A. acknowledges ICREA Academia, and the Joint Appointment Program at PNNL. PNNL is a multiprogram national laboratory operated for the U.S. Department of Energy (DOE) by Battelle Memorial Institute under Contract No. DE-AC0576RL01830. The project has also received funding from the European Union's Horizon 2020 research and innovation program under the Marie Sklodowska-Curie Grant Agreement No. 945413 and from the Universitat Rovira i Virgili (URV). D.S.P. acknowledges financial support through Grants No. JDC2022-048339-I and No. PID2021-128005NB-C21 funded by MCIN/AEI/10.13039/501100011033 and the European Union "NextGenerationEU"/PRTR."

M.M., D.S.P., and A.A. designed the study. M.M. and M.H. wrote code. M.M. wrote equations and performed the analysis. All the authors analyzed results, discussed results, and wrote the paper.

The authors declare no competing financial interests.

DATA AVAILABILITY

No data were created or analyzed in this study.

[1] O. X. Cordero and M. S. Datta, Microbial interactions and community assembly at microscales, Curr. Opin. Microbiol. **31**, 227 (2016).

[2] J. L. M. Welch, B. J. Rossetti, C. W. Rieken, F. E. Dewhirst, and G. G. Borisy, Biogeography of a human oral microbiome at the micron scale, Proc. Natl. Acad. Sci. USA **113**, E791 (2016).

[3] R. Sheth, M. Li, and W. Jiang *et al.*, Spatial metagenomic characterization of microbial biogeography in the gut, Nat. Biotechnol. **37**, 877 (2019).

[4] S. L. O'Brien, S. M. Gibbons, S. M. Owens, J. Hampton-Marcell, E. R. Johnston, J. D. Jastrow, J. A. Gilbert, F. Meyer, and D. A. Antonopoulos, Spatial scale drives patterns in soil bacterial diversity, Environ. Microbiol. **18**, 2039 (2016).

[5] E. Bar-Zeev, I. Berman-Frank, O. Girshevitz, and T. Berman, Revised paradigm of aquatic biofilm formation facilitated by microgel transparent exopolymer particles, Proc. Natl. Acad. Sci. USA **109**, 9119 (2012).

[6] O. Hallatschek, P. Hersen, S. Ramanathan, and D. R. Nelson, Genetic drift at expanding frontiers promotes gene segregation, Proc. Natl. Acad. Sci. USA **104**, 19926 (2007).

[7] I. Golding, I. Cohen, and E. Ben-Jacob, Studies of sector formation in expanding bacterial colonies, Europhys. Lett. **48**, 587 (1999).

[8] E. Budrene and H. Berg, Complex patterns formed by motile cells of *Escherichia coli*, Nature (London) **349**, 630 (1991).

[9] C. M. Waters and B. L. Bassler, Quorum sensing: Cell-to-cell communication in bacteria, Annu. Rev. Cell Dev. Biol. **21**, 319 (2005).

[10] R. Daniels, J. Vanderleyden, and J. Michiels, Quorum sensing and swarming migration in bacteria, FEMS Microbiol. Rev. **28**, 261 (2004).

[11] H. H. Hoang, N. Gurich, and J. E. González, Regulation of motility by the ExpR/Sin quorum-sensing system in *Sinorhizobium meliloti*, J. Bacteriol. **190**, 861 (2008).

[12] R. F. Kinsinger, M. C. Shirk, and R. Fall, Rapid surface motility in *Bacillus subtilis* is dependent on extracellular surfactin and potassium ion, J. Bacteriol. **185**, 5627 (2003).

[13] G. Cárcamo-Oyarce, P. Lumjiaktase, R. Kümmerli *et al.*, Quorum sensing triggers the stochastic escape of individual cells from *Pseudomonas putida* biofilms, Nat. Commun. **6**, 5945 (2015).

[14] R. Daniels, S. Reynaert, H. Hoekstra, C. Verreth, J. Janssens, K. Braeken, M. Fauvart, S. Beullens, C. Heusdens, I. Lambrichts, D. E. D. Vos, J. Vanderleyden, J. Vermant, and J. Michiels, Quorum signal molecules as biosurfactants affecting swarming in *Rhizobium etli*, Proc. Natl. Acad. Sci. USA **103**, 14965 (2006).

[15] J. Tailleur and M. E. Cates, Statistical mechanics of interacting run-and-tumble bacteria, Phys. Rev. Lett. **100**, 218103 (2008).

[16] M. E. Cates and J. Tailleur, Motility-induced phase separation, Annu. Rev. Condens. Matter Phys. **6**, 219 (2015).

[17] Y. Fily and M. C. Marchetti, Athermal phase separation of self-propelled particles with no alignment, Phys. Rev. Lett. **108**, 235702 (2012).

[18] G. S. Redner, M. F. Hagan, and A. Baskaran, Structure and dynamics of a phase-separating active colloidal fluid, Phys. Rev. Lett. **110**, 055701 (2013).

[19] A. Curatolo, N. Zhou, Y. Zhao *et al.*, Cooperative pattern formation in multi-component bacterial systems through reciprocal motility regulation, Nat. Phys. **16**, 1152 (2020).

[20] W. J. M. Ridgway, M. P. Dalwadi, P. Pearce, and S. J. Chapman, Motility-induced phase separation mediated by bacterial quorum sensing, Phys. Rev. Lett. **131**, 228302 (2023).

[21] A. Dinelli, J. O'Byrne, A. Curatolo *et al.*, nonreciprocity across scales in active mixtures, Nat. Commun. **14**, 7035 (2023).

[22] Y. Duan, J. Agudo-Canalejo, R. Golestanian, and B. Mahault, Dynamical pattern formation without self-attraction in quorum-sensing active matter: The interplay between nonreciprocity and motility, Phys. Rev. Lett. **131**, 148301 (2023).

[23] A. Dinelli, A. Altieri, and J. Tailleur, Random motility regulation drives the fragmentation of microbial ecosystems, arXiv:2503.12692.

[24] M. Mattei and A. Arenas, Exploring spatial segregation induced by competition avoidance as driving mechanism for emergent coexistence in microbial communities, Phys. Rev. E **110**, 014404 (2024).

[25] See Supplemental Material at http://link.aps.org/supplemental/10.1103/g5bm-m9c4 for spatial organization and cluster size distributions; hysteresis curve and clusters stability; sensitivity analysis; parameters choice and simulation details, which also includes Refs. [56,57].

[26] G. J. Tortora, B. R. Funke, and C. L. Case, *Microbiology: An Introduction* (Benjamin Cummings, Redwood City, CA, 1995), p. 275.

[27] *The World Book Encyclopedia* (Field Enterprises, Chicago, 1973), p. 18.

[28] K. F. Kelton and A. L. Greer, *Nucleation in Condensed Matter: Applications in Materials and Biology*, Pergamon Materials Series Vol. 15 (Elsevier, Oxford, UK, 2010).

[29] D. W. Oxtoby, Homogeneous nucleation: Theory and experiment, J. Phys.: Condens. Matter **4**, 7627 (1992).

[30] F. Peruani, A. Deutsch, and M. Bär, Nonequilibrium clustering of self-propelled rods, Phys. Rev. E **74**, 030904(R) (2006).

[31] D. T. Gillespie, Exact stochastic simulation of coupled chemical reactions, J. Phys. Chem. **81**, 2340 (1977).

[32] P. Erdős and A. Rényi, On random graphs. I, Publ. Math. Debrecen **6**, 290 (1959).

[33] A.-L. Barabási and R. Albert, Emergence of scaling in random networks, Science **286**, 509 (1999).

[34] P. W. Holland, K. B. Laskey, and S. Leinhardt, Stochastic blockmodels: First steps, Social Networks **5**, 109 (1983).

[35] V. M. Worlitzer, A. Jose, I. Grinberg, M. Bär, S. Heidenreich, A. Eldar, G. Ariel, and A. Be'er, Biophysical aspects underlying the swarm to biofilm transition, Sci. Adv. **8**, eabn8152 (2022).

[36] D. G. Davies, M. R. Parsek, J. P. Pearson, B. H. Iglewski, J. W. Costerton, and E. P. Greenberg, The involvement of cell-to-cell signals in the development of a bacterial biofilm, Science **280**, 295 (1998).

[37] D. López, M. A. Fischbach, F. Chu, R. Losick, and R. Kolter, Structurally diverse natural products that cause potassium leakage trigger multicellularity in *Bacillus subtilis*, Proc. Natl. Acad. Sci. USA **106**, 280 (2009).

[38] E. Ben-Jacob, O. Schochet, A. Tenenbaum *et al.*, Generic modeling of cooperative growth patterns in bacterial colonies, Nature (London) **368**, 46 (1994).

[39] J. Tyler Bonner and L. J. Savage, Evidence for the formation of cell aggregates by chemotaxis in the development of the slime mold *Dictyostelium discoideum*, J. Exp. Zool. **106**, 1 (1947).

[40] J. Agudo-Canalejo and R. Golestanian, Active phase separation in mixtures of chemically interacting particles, Phys. Rev. Lett. **123**, 018101 (2019).

[41] X. Diego, L. Marcon, P. Müller, and J. Sharpe, Key features of Turing systems are determined purely by network topology, Phys. Rev. X **8**, 021071 (2018).

[42] R. May, Will a large complex system be stable? Nature (London) **238**, 413 (1972).

[43] S. Allesina and S. Tang, Stability criteria for complex ecosystems, Nature (London) **483**, 205 (2012).

[44] K. Faust and J. Raes, Microbial interactions: From networks to models, Nat Rev Microbiol **10**, 538 (2012).

[45] A. Barberán, S. Bates, E. Casamayor *et al.*, Using network analysis to explore co-occurrence patterns in soil microbial communities, ISME J **6**, 343 (2012).

[46] T. P. Peixoto, Network reconstruction via the minimum description length principle, Phys. Rev. X **15**, 011065 (2025).

[47] J. E. Goldford, N. Lu, D. Bajić, S. Estrela, M. Tikhonov, A. Sanchez-Gorostiaga, D. Segrè, P. Mehta, and A. Sanchez, Emergent simplicity in microbial community assembly, Science **361**, 469 (2018).

[48] A. Zelezniak, S. Andrejev, O. Ponomarova, D. R. Mende, P. Bork, and K. R. Patil, Metabolic dependencies drive species co-occurrence in diverse microbial communities, Proc. Natl. Acad. Sci. USA **112**, 6449 (2015).

[49] A. Dal Co, S. van Vliet, D. Kiviet *et al.*, Short-range interactions govern the dynamics and functions of microbial communities, Nat. Ecol. Evol. **4**, 366 (2020).

[50] X. Raynaud and N. Nunan, Spatial ecology of bacteria at the microscale in soil, PLOS ONE **9**, e87217 (2014).

[51] J. van Gestel, T. Bareia, B. Tenennbaum *et al.*, Short-range quorum sensing controls horizontal gene transfer at micron scale in bacterial communities, Nat. Commun. **12**, 2324 (2021).

[52] K. Drescher, J. Dunkel, C. D. Nadell, S. van Teeffelen, I. Grnja, N. S. Wingreen, H. A. Stone, and B. L. Bassler, Architectural transitions in *Vibrio cholerae* biofilms at single-cell resolution, Proc. Natl. Acad. Sci. USA **113**, E2066 (2016).

[53] Z. You, D. J. G. Pearce, A. Sengupta, and L. Giomi, Mono- to multilayer transition in growing bacterial colonies, Phys. Rev. Lett. **123**, 178001 (2019).

[54] https://mathworld.wolfram.com/Circle-CircleIntersection.html.

[55] M. Penrose, *Random Geometric Graphs*, *Oxford Studies in Probability* (Oxford University Press, Oxford, 2003), Vol. 5.

[56] *McGraw-Hill Encyclopedia of Science and Technology* (McGraw Hill, New York, 1960), p. 63.

[57] C. Spearman, The proof and measurement of association between two things, Am. J. Psychol. **15**, 72 (1904).